






The adaptive roles of aneuploidy and polyclonality in *Leishmania* in response to environmental stress

Gabriel H Negreira¹ , Robin de Groot¹, Dorien Van Giel¹, Pieter Monsieurs¹ , Ilse Maes¹, Geraldine de Muylder¹, Frederik Van den Broeck^{1,2} , Jean-Claude Dujardin^{1,3}  & Malgorzata A Domagalska^{1,*} 

Abstract

Aneuploidy is generally considered harmful, but in some microorganisms, it can act as an adaptive mechanism against environmental stress. Here, we use *Leishmania*—a protozoan parasite with remarkable genome plasticity—to study the early steps of aneuploidy evolution under high drug pressure (using antimony or miltefosine as stressors). By combining single-cell genomics, lineage tracing with cellular barcodes, and longitudinal genome characterization, we reveal that aneuploidy changes under antimony pressure result from polyclonal selection of pre-existing karyotypes, complemented by further and rapid *de novo* alterations in chromosome copy number along evolution. In the case of miltefosine, early parasite adaptation is associated with independent point mutations in a miltefosine transporter gene, while aneuploidy changes only emerge later, upon exposure to increased drug levels. Therefore, polyclonality and genome plasticity are hallmarks of parasite adaptation, but the scenario of aneuploidy dynamics depends on the nature and strength of the environmental stress as well as on the existence of other pre-adaptive mechanisms.

Keywords adaptation; aneuploidy; cellular barcodes; *Leishmania*; single-cell genomics

Subject Categories Chromatin, Transcription & Genomics; Evolution & Ecology; Microbiology, Virology & Host Pathogen Interaction

DOI 10.15252/embr.202357413 | Received 28 April 2023 | Revised 15 June 2023 | Accepted 30 June 2023 | Published online 20 July 2023

EMBO Reports (2023) 24: e57413

Introduction

Aneuploidy, that is, a dosage imbalance between chromosomes in a cell, is commonly lethal or associated with deleterious effects, in particular in multicellular organisms (Ricke & van Deursen, 2013; Chunduri & Storchová, 2019). In some unicellular eukaryotes however, aneuploidy can be well-tolerated or even beneficial. It can be found in pathogenic and non-pathogenic unicellular eukaryotes,

including *Saccharomyces cerevisiae*, *Candida albicans*, *Cryptococcus neoformans*, and *Giardia intestinalis* (Mulla *et al*, 2014; Tůmová *et al*, 2016; Yang *et al*, 2021), with specific aneuploidy changes being able to confer resistance against environmental stresses such as drug pressure (Yang *et al*, 2019). Additionally, aneuploidy is also a hallmark of cancer, where it is associated with the therapeutic resistance, either by promoting dosage changes of key genes or by causing delays in drug-targeted cell cycle stages (Replogle *et al*, 2020; Ippolito *et al*, 2021).

In recent years, *Leishmania* spp. emerged as a unique model for studying aneuploidy and its adaptive role. These protozoan parasites cause leishmaniases and display a digenetic life cycle characterized by two main forms: the extracellular promastigote in the midgut lumen of female sand flies, and the amastigote in phagocytic cells of the vertebrate hosts (Mann *et al*, 2021). *Leishmania* spp. display several idiosyncratic genomic and molecular features compared to other eukaryotes. Their genomes lack gene-specific RNAPol II promoters and are organized in long polycistronic arrays encompassing hundreds of genes which are not functionally related (Clayton, 2019). Transcription is thus initiated at defined chromosomal locations known as strand switch regions, which flank the polycistrons. In this context, gene dosage has a nearly one-to-one impact on transcription (Dumetz *et al*, 2017) and directly affect gene expression, which otherwise is mainly controlled post-transcriptionally.

Unlike the abovementioned organisms where euploid genomes are common, all *Leishmania* genomes analyzed hitherto are aneuploid, with the most basic profile being characterized by a polysomy in chromosome 31, contrasting with a disomy in the other 33–35 chromosomes (Rogers *et al*, 2011; Mannaert *et al*, 2012). Additional dosage changes affecting multiple chromosomes (up to 22 out of 36 chromosomes) are commonly observed in cultured promastigotes (Imamura *et al*, 2016) and are associated with a fitness gain *in vitro* (Bussotti *et al*, 2018, 2021), but they also occur—to a lower extent—in amastigotes, *in vivo* (Domagalska *et al*, 2019). Recently, a multi-omics study demonstrated a proportional impact of polysomies on the average expression of proteins encoded by the respective polysomic chromosomes, ultimately correlated with

¹ Molecular Parasitology Unit, Institute of Tropical Medicine Antwerp, Antwerp, Belgium

² Department of Microbiology, Immunology and Transplantation, Rega Institute for Medical Research, Katholieke Universiteit Leuven, Leuven, Belgium

³ Department of Biomedical Sciences, University of Antwerp, Antwerp, Belgium

*Corresponding author. Tel: +32 32476596; E-mail: mdomagalska@itg.be

metabolic adaptations (Cuypers *et al.*, 2022). Moreover, aneuploidy in *Leishmania* is highly dynamic and changes in response to new environments, such as drug pressure, vertebrate host or vector (Dumetz *et al.*, 2017, 2018). Interestingly, spontaneous karyotypic modifications constantly occur even among sister cells in clonal populations, a phenomenon known as mosaic aneuploidy (Sterkers *et al.*, 2011; Negreira *et al.*, 2021). It is postulated that mosaic aneuploidy in *Leishmania* leads to phenotypic heterogeneity that can serve as substrate for natural selection, facilitating adaptation to different environmental pressures (Sterkers *et al.*, 2012), but this remains an open question. Moreover, the clonal dynamics of populations facing strong environmental stresses and its relationship with aneuploidy modifications are currently unknown.

In the present study, we aimed to address these questions using a reproducible *in vitro* evolutionary model to study karyotype evolution in the context of early adaptation to sudden environmental stresses, invoked here by the direct exposure to high concentrations of two drugs, trivalent antimonial (Sb^{III}) or miltefosine (further called ‘flash selection’). By combining single-cell genome sequencing (SCGS), clonal lineage tracing with cellular barcodes and longitudinal genomic characterization, we showed that changes in aneuploidy under Sb^{III} pressure arise from the polyclonal selection of pre-existing karyotypes which converge to similar aneuploidy profiles through further cumulative karyotypic alterations. In contrast, adaptation to miltefosine was initially driven by the polyclonal selection of distinct missense mutations in a miltefosine transporter gene (LdMT), with aneuploidy modifications only happening after the already-selected populations were exposed to a 4 times higher dosage. Thus, the dynamics of aneuploidy modulations is contingent upon the specific environmental stressors, their intensity, and the presence of other pre-adaptive mechanisms.

Results and Discussion

In the present study, we investigated the mechanisms governing the early adaptation of *Leishmania* promastigotes by directly exposing a *L. donovani* promastigote clonal strain (BPK282) to a high concentration of Sb^{III} (382 μ M) or miltefosine (25–100 μ M) *in vitro*. For each model—which we refer as ‘flash selection’—we followed two molecular approaches: (i) bulk and SCGS, with a special focus on aneuploidy and (ii) lineage tracing with cellular barcodes (Fig EV1A and B). This allowed us to track the evolutionary dynamics of hundreds of lineages under drug pressure, revealing the bottlenecks associated with each model and the relationship between selection of lineages and the emergence of genomic adaptations.

Flash selection with Sb^{III} leads to rapid changes in aneuploidy

The first flash selection protocol we used was previously developed in a study on resistance to trivalent antimonial (Sb^{III}), in which resistant parasites with fully restored growth to wild-type levels were observed after 5 weeks (and passaged every 7 days) of direct exposure to 382 μ M Sb^{III} (Dumetz *et al.*, 2018). We reproduced the experiment with a barcoded BPK282 and determined by bulk whole genome sequencing (WGS) the genomic alterations encountered in the populations along five passages under Sb^{III} pressure and in four replicates (further called SePOP1-4). The search for SNPs and indels

in coding regions did not reveal any consistent change associated with the Sb^{III} pressure compared to the control populations (cPOP1-4) which were maintained with PBS in place of Sb^{III} (Fig EV2A). We also evaluated intrachromosomal copy number variations with a specific attention for the MRPA gene (chromosome 23) which encodes an ABC transporter involved in Sb^{III} sequestration (Frézard *et al.*, 2014) that is often amplified in Sb^{III} resistant *Leishmania* (Dumetz *et al.*, 2018). In 3 out of 4 replicates, the copy number of the MRPA locus remained stable at ~ 3 copies per haploid genome similarly to the initial condition as well as to cPOP1-4, with the exception of SePOP1, which displayed an increase to almost 10 copies per haploid genome at passage 5 (Fig EV2B). When investigating aneuploidy variation, we found that BPK282 contained six chromosomes with some higher than 2 (chr 5, 9, 16, 23, 26, and 31) at the onset of the experiment, and we found a further dosage increase affecting 5–8 chromosomes at passages 2–3 in SePOP1-4 after Sb^{III} exposure (Fig 1A). Interestingly, although distinct aneuploidy profiles emerged in different replicates, all four replicates consistently shared a dosage increase of chromosomes 23, 27, and 31, which could point to an adaptive advantage of the amplification of these chromosomes.

The dosage increase of these chromosomes, in particular chromosome 23, is commonly reported in several antimony resistance studies, including in other *L. donovani* strains (Dumetz *et al.*, 2018) as well as other *Leishmania* species such as *L. infantum*, *L. guyanensis*, *L. braziliensis*, and *L. panamensis* (Brotherton *et al.*, 2013; Montenegro *et al.*, 2015; Patino *et al.*, 2019). The line here used (BPK282) is remarkably pre-adapted to Sb^{III} (Dumetz *et al.*, 2018)—like other strains of the Gangetic plain—thanks to a pre-existing intrachromosomal amplification of MRPA genes encountered in 200 sequenced *L. donovani* isolates of that region (Imamura *et al.*, 2016). This pre-adaptation likely comes from the combination of high antimony pressure for decades, highly endemic pollution with arsenic—which can cause cross-resistance to antimonials (Perry *et al.*, 2011, 2013)—and anthroponotic transmission without animal reservoir. The recurrent dosage increase of chromosome 23 observed here under Sb^{III} pressure is thus a rapid way to further amplify the MRPA gene. Noteworthy, even in parasites in which MRPA was artificially deleted, chromosome 23 still consistently displayed increase in copy number in populations selected for antimony resistance, suggesting that other genes in this chromosome beyond MRPA might be relevant to antimony tolerance (Douanne *et al.*, 2020).

Regarding the other two chromosomes, chromosome 31 also bears a gene involved in antimony resistance, the sodium stibogluconate resistance protein gene (LdBPK_310951.1). Interestingly, the ortholog of this gene displayed an increased copy number in *L. braziliensis* promastigotes experimentally selected for antimony resistance *in vitro* compared to non-selected lines (Patino *et al.*, 2019). Moreover, this same study found a 50 kb intrachromosomal amplification affecting 23 genes (out of a total of 31 amplified genes) in chromosome 27 in the Sb^{III} resistant line, with many of these genes displaying a copy number more than 10 times higher compared to the Sb^{III} sensitive line (Patino *et al.*, 2019). Among these genes, a WW domain/Zinc finger CCCH type-protein gene (LdBPK_270130.1 ortholog in *L. donovani*) was also the gene with the most upregulated expression compared to the Sb^{III}-sensitive line. Importantly, CCCH type zinc finger proteins are known targets of antimony (Frézard *et al.*, 2014), and therefore, a higher expression of this gene might mitigate its inactivation by the drug.

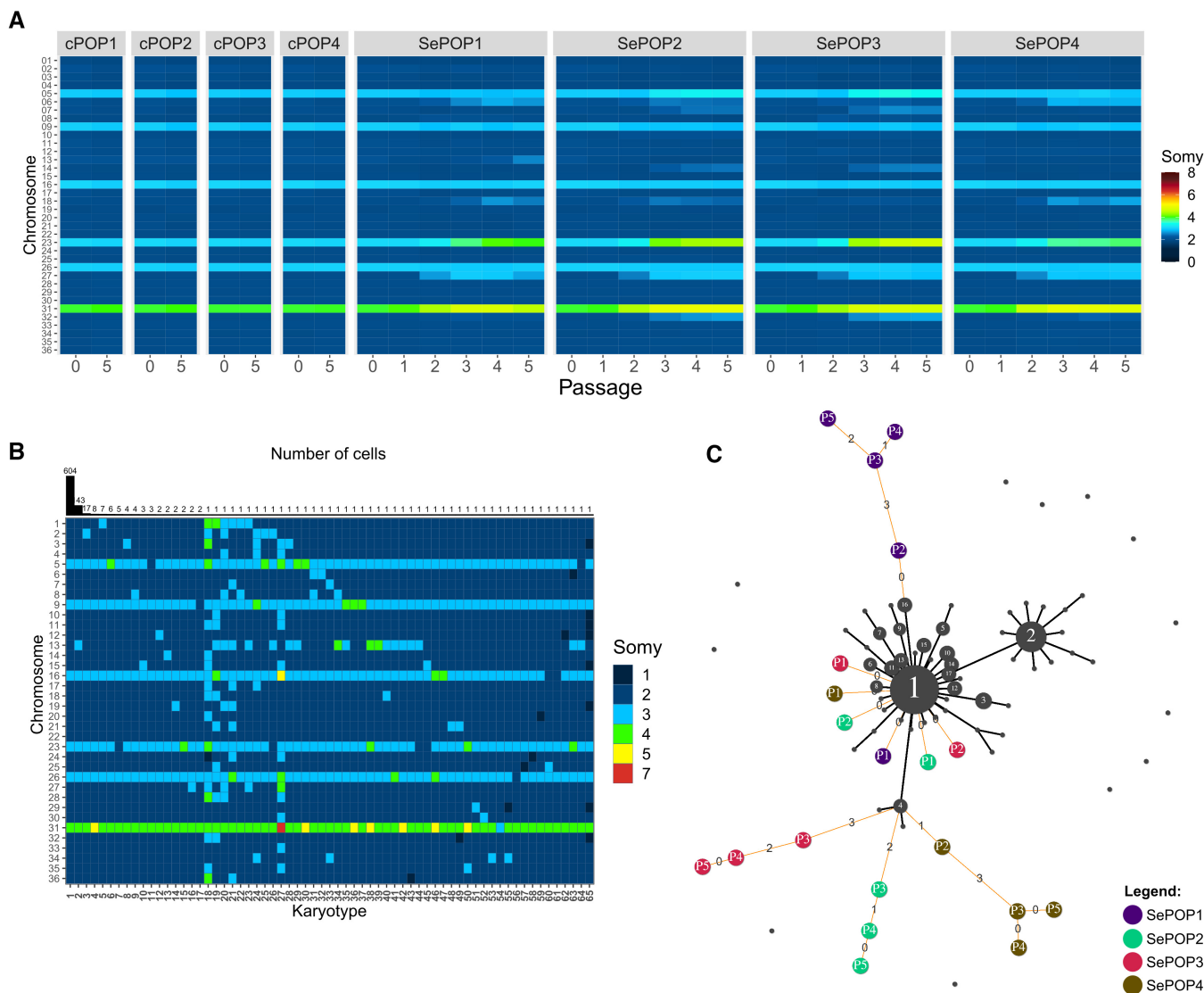


Figure 1. Aneploidy changes of *L. donovani* BPK282 during flash selection with Sb^{III}.

A Bulk genome sequencing: Heatmap showing the average copy number of each chromosome between passages 0 (before drug exposure) and passage 5 in cPOP1-4 and along all 5 passages in the four replicates under Sb^{III} flash selection (SePOP1-4).

B Heatmap depicting all karyotypes identified in the barcoded population prior to Sb^{III}-exposure using SCGS. Karyotypes are ordered decreasingly based on their frequency. Bars on the top display the number of promastigotes found with each karyotype.

C Minimum spanning tree displaying the number of somy changes between the karyotypes identified in the single-cell data (black nodes) and the rounded bulk aneuploidy of the Sb^{III}-selected populations (colored nodes: purple = SePOP1, green = SePOP2, red = SePOP3 and brown = SePOP4) at passages 1-5 (P1-P5); we based this analysis on the previous observation that the rounded bulk aneuploidy profile of a given promastigote population reflects the most dominant karyotype in that population (Negreira et al, 2021). Black lines connecting two nodes indicate that these two karyotypes are different by a single somy change. Orange lines connect the bulk karyotypes of the SePOP1-4 to the single-cell data. Numbers in the orange lines indicate how many somy changes are between the nodes connected by them. Unconnected black nodes are single-cell karyotypes that have 2 or more somy differences compared to any other karyotype.

Source data are available online for this figure.

Single-cell genomics reveals potential evolutionary paths that led to Sb^{III}-associated aneploidy changes

To evaluate if the aneploidy changes observed in the Sb^{III}-exposed populations are due to the selection of pre-existing or *de novo* generated karyotypes, we submitted the same barcoded cell population to high throughput SCGS prior to flash selection. In total, 864

promastigotes were individually sequenced, with a total of 65 different karyotypes (kar1-65) being detected (Fig 1B). These single-cell data revealed a relatively reduced mosaicism, with almost 70% of the parasites displaying the same karyotype (kar1). None of the pre-existing karyotypes were identical to the aneploidy profiles observed in bulk in SePOP1-4 (Fig 1B). However, individual somy changes consistently observed in SePOP1-4 (tetrasomy in chromosome 23, trisomy in

chromosome 27 and pentasomy in chromosome 31) were already present—in few cells—before the flash selection. For instance, kar18—one of the most aneuploid karyotypes, had a tetrasomic chromosome 23 and a trisomic chromosome 27, while kar38 and kar50 both shared amplification of chromosome 23 and 31. Other single cells showed dosage increase of one of these chromosomes only, for instance, kar15 that only showed tetrasomy of chromosome 23. However, none of the sequenced promastigotes showed amplification of chromosomes 23, 27, and 31 concomitantly, and no pre-existing karyotype was identified with a pentasomy in chromosome 23 as observed in the SePOP3, suggesting that some of the aneuploidy changes seen in SePOP1-4 happened either after initial exposure to Sb^{III} or that they were present at a frequency lower than the detection limit of our SCS data (1 in 864 or 0.116%).

To gain insights on possible evolutionary paths leading to the aneuploidy changes observed in the SePOP1-4 (bulk data) from the initial population (single-cell data), we built a minimum spanning tree connecting the karyotypes found in the single-cell data (Fig 1C—black nodes) to the rounded aneuploidy profiles of SePOP1-4 (Fig 1C—colored nodes). This approach revealed that the shortest path between pre-existing karyotypes and the selected karyotypes in SePOP1 starts from kar16, which has the same aneuploidy profile as the one observed in this population at passage 2, characterized by a trisomic chromosome 27. For SePOP2-4, the closest pre-existing karyotype is kar4, which has a pentasomic chromosome 31. At passage 2, SePOP4 is almost identical to kar4, being one step away from this karyotype. This single somy difference is due to a trisomy in chromosome 27 which is not present in kar4. From passage 2–3, SePOP4 accumulated 3 extra somy changes (trisomy in chromosomes 6 and 18 and a tetrasomy in chromosome 23). For SePOP2 and SePOP3, the first aneuploidy changes emerged at passage 3 and had already 2 and 3 somy differences compared to kar4, respectively. Thus, the tree points to a process of polyclonal selection of subpopulations bearing pre-existing chromosomal amplifications followed by cumulative karyotypic modifications in subsequent time points in SePOP1-4.

Changes in aneuploidy in Sb^{III} selection arise from polyclonal selection and convergent evolution

To document the cell population dynamics during adaptation to Sb^{III}, we applied cellular barcodes to track the evolution of hundreds

of clonal lineages during flash selection. In summary, we generated a barcoded promastigote population consisting of 453 different traceable lineages. The frequency of each lineage in each SePOP was monitored by amplicon sequencing. This approach revealed that the flash selection with Sb^{III} led to a fourfold reduction in lineage diversity that stabilized between passages 3 and 4, leaving between 101 and 131 of detectable lineages (Fig EV3A).

To distinguish frequency changes associated with Sb^{III} pressure from other sources of variation, such as stochastic loss due to passaging, we normalized the frequency of each lineage in each SePOP to their respective average frequency in the cPOP at each passage (Fig 2A). Here we refer to this parameter as “Sb^{III}-associated frequency change”. In this sense, lineages that, for example, die or are negatively affected under antimony pressure but not under standard *in vitro* conditions display a negative Sb^{III}-associated frequency change, while lineages that are eliminated over time in both cPOP and SePOP display similar values. This analysis showed that a large fraction of lineages representing a total 74.6–84.8% of the initial population was negatively affected or completely eliminated during Sb^{III} pressure (Fig 2B). This fraction was represented by a total of 362–395 lineages, including 303 which were consistently affected negatively in all four SePOP (Fig 2C, left panel, red), suggesting that this subset of lineages had a lower tolerance to Sb^{III} stress. Interestingly, the fraction of positively affected lineages represented 5.2–8.4% of the initial population (Fig 2B), with only 60 lineages displaying a frequency higher in the drug-exposed group compared to the controls at passage 5. This subset became dominant to represent 77.7–97.4% of the final populations at passage 5. Moreover, most of the positively affected lineages were enriched in only one of the SePOPs (Figs 2C and EV3B). Altogether, these data suggest that (i) a subset of lineages was fitter to Sb^{III} prior to the drug exposure and (ii) the further expansion of these surviving lineages was divergent between independent replicates.

In an attempt to link the evolution of lineages as revealed by barcoding sequencing with the aneuploidy modifications observed in the bulk WGS of SePOP1-4, we processed each dataset with a ‘trajectory’ principal component analysis (PCA) and compared them (Fig 2D and E). The former one revealed that lineage composition progressively diverged between replicates, with SePOP1/4 deviating further from SePOP2/3 at later passages (Fig 2D). Interestingly, this PCA based on lineage composition resembled the aneuploidy-based PCA shown in Fig 2E, with SePOP1/4 and 2/3 clustering separately,

Figure 2. Clonal dynamics of Sb^{III} adaptation revealed with cellular barcodes.

- Fold-change of the frequency of each clone in the Sb^{III}-exposed group (4 replicates—SePOP1-4) relative to their average frequency in the control group in the same time point (Sb^{III}-associated fold change). Each dot represents a barcoded lineage. Lineages with a log₂ Sb^{III}-associated fold change smaller than -2 or greater than +2 were considered negatively and positively affected respectively. Lineages with fold-change at -infinite are lineages that were eliminated under drug pressure.
- Fraction of lineages that by passage 5 were either positively affected (red) or negatively affected (blue) by Sb^{III} pressure.
- Evaluation of the consistency of the Sb^{III}-associated fold change scores among replicates. The bars represent the proportion of clones that had a particular Sb^{III}-associated fold-change effect (higher, lower or same as in control) in 1, 2, 3, or 4 replicates (dark blue, light blue, orange, and red, respectively). The numbers in the bars indicate the absolute number of barcodes.
- Trajectory principal component analysis (PCA) of the changes in clonal composition over time in each population. This was done by performing a regular PCA on each dataset and connecting the data points of each population with an arrow line indicating their trajectories from passage 0 to passage 5. The PCA was based on the frequency of each lineage identified in each sample. The numbers indicate the passages at which each sample was collected, while colors indicate the populations.
- Trajectory PCA depicting the changes in aneuploidy in all samples. Numbers indicate the passage number at which a sample was collected for WGS. Due to strong similarity between controls, they are not well visible in the PCAs as they cluster very close to each other.
- Frequency of each barcoded lineage along the five passages under Sb^{III} pressure (top panel). Only barcodes that reached frequencies higher than 1% at passage 5 in at least one of the replicates were colored. A repetition of Fig 1A is included for comparison (bottom panel).

Source data are available online for this figure.

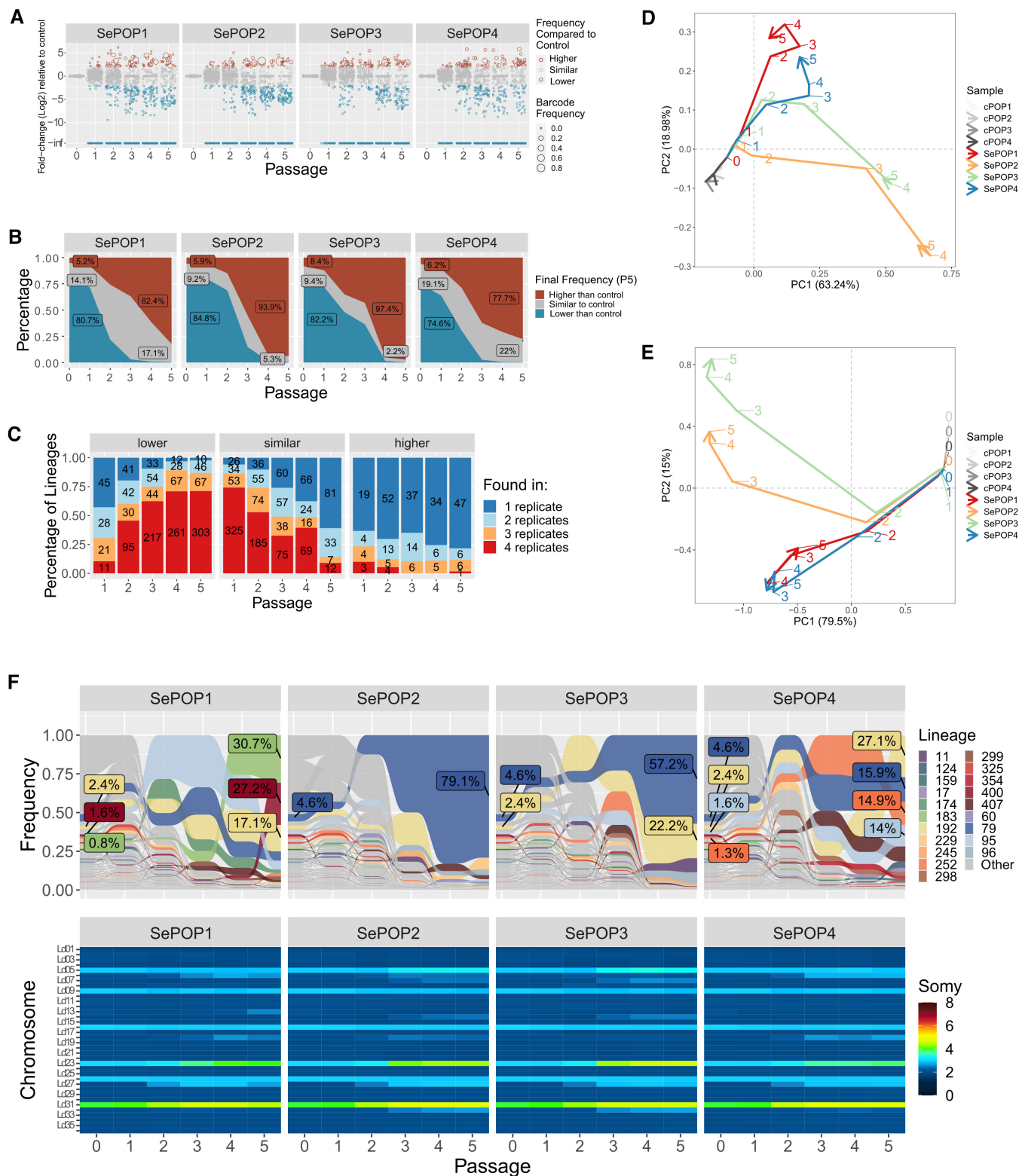


Figure 2.

suggesting that changes in aneuploidy coincide with changes in lineage composition. This observation is supported when comparing the absolute frequency of the lineages with the aneuploidy changes

observed in bulk at each timepoint (Figs 2F and EV3C). Here we observe that the major aneuploidy alterations arise at passages 2 to 3, coinciding with the moment where the most dominant lineages in

the initial population are depleted while other lineages expand. It is also noticeable that the aneuploidy changes in SePOP2/3 are almost identical, and these two populations were dominated by the same lineage (lineage 79). Conversely, SePOP1/4 also share similar aneuploidy changes, though different from replicates 2 and 3, but lineage composition seems to be less similar. In addition, the lineage tracing data also indicated that lineages that were selected under Sb^{III} exposure were already at frequencies above the detection limit of our SCGS data (see Fig 2F, passage 0). Thus, the most likely explanation for the aneuploidy changes seen in the bulk WGS data of SePOP1-4 is that the karyotypes selected under drug pressure indeed originated from pre-existing karyotypes but underwent further and rapid cumulative changes in chromosome number under Sb^{III} pressure. Moreover, the observation that the same set of three chromosomes displayed dosage increases in all SePOP despite the fact that different lineages dominated each SePOP points to a process of convergent evolution which further supports the notion of these chromosomes being under positive selection.

Adaptation to miltefosine is associated with polyclonal selection of nucleotide variants

The results described above demonstrated the importance of aneuploidy for parasite adaptation to high Sb^{III} pressure together with the polyclonality of corresponding molecular adaptations. In the next step, we investigated whether the same mechanisms would be associated with adaptation to another anti-*Leishmania* drug: miltefosine. Noteworthy, BPK282 was isolated from the main population endemic in the Gangetic plain, before miltefosine was implemented in the region (in sharp contrast to Sb^{III}). Hence, different results were expected for the scenario of genomic adaptation and clonal dynamics. In contrast to Sb^{III}, there was—at least before present study—no pre-adaptation known to miltefosine in the BPK282 strain, which is considered very susceptible to the drug (Shaw *et al*, 2016).

In order to initiate a flash selection with miltefosine, we first determined which was the highest concentration of the drug in which viable parasites could still be recovered: four replicates were considered per condition (MIL-exposed populations, MePOP1-4; Fig EV4A). The cultures with 50 and 100 μ M of miltefosine did not display live parasites even after 1 month post addition of the drug (no passaging). However, in the cultures with 25 μ M of MIL, although no live parasites could be detected by microscopy until the 10th day, viable promastigotes started to arise afterwards, and by the 17th day post addition of MIL, MePOP1-4 displayed a relative cell density comparable to the controls as estimated by microscopy. These populations of survivors displayed such a higher tolerance to miltefosine that an attempt to determine their IC₅₀ against the drug was not successful as the cultures did not suffer a reduction in

viability even in the highest concentration used in the test (75 μ M—Fig EV4B). Their respective IC₅₀s were determined at passage 2 by including an additional concentration of 150 μ M in the test and was defined as an average of 81.78 μ M in MePOP1-4 and 21.9 μ M in the control group ($P < 0.001$, t -test—Fig EV4C).

When looking for genomic changes using bulk WGS, we found that the strong bottleneck associated with miltefosine exposure did not lead to any major alteration in aneuploidy, as MePOP1-4 displayed the same profile as the initial population even after nine passages under miltefosine pressure at 25 μ M (Fig 3A). However, subsequent exposure of the MePOPs to 100 μ M for four passages did lead to drastic changes in aneuploidy affecting several chromosomes (Fig 3A). This demonstrated that the strong bottleneck induced by miltefosine in the first passage did not impair the potential for aneuploidy modulations in later passages and that these modifications depend on the strength of the stress caused by the drug. These observations are also in agreement with the notion of aneuploidy modulations happening *de novo* during adaptation to the drug as the aneuploidy profiles seen at passage 9 in the MePOPs exposed to 100 μ M are also very different from the pre-existing karyotypes identified in the single-cell data of BPK282. In each MePOP a different profile was seen, although 3 out of 4 shared the amplification of chromosome 31, and two MePOPs displayed a dosage increase in chromosome 23. The fact that an increase in copy number of chromosome 31 was observed under strong Sb^{III} and miltefosine pressure, as well as under pressure of other drugs (Hefnawy *et al*, 2022) might indicate that the dosage increase in this chromosome has also a general role against multiple types of stresses. Noteworthy, there are several ABC transporters in that chromosome (ABCC4-7 and ABCD3) which could play a role in drug efflux (Leprohon *et al*, 2006). Moreover, ontology analysis of chromosome 31 in *L. braziliensis* demonstrated an enrichment of genes involved in iron metabolism which could play a role in general adaptation to oxidative stresses (Valdivia *et al*, 2015), but empirical evidence is still lacking.

In contrast to the Sb^{III} model, relevant SNPs were encountered between MePOP1-4 and the controls, already from the first passage. In particular, in the four selected populations, independent missense mutations arose in the phospholipid-transporting ATPase1-likeprotein gene, which is also known as the miltefosine transporter (LdMT—ID: LdBPK_131590.1). In MePOP1, 3 and 4 the same mutation promoting a substitution of a glycine by an aspartate at amino acid (Gly160Asp) was observed, while MePOP2 displayed a different mutation in the same gene leading to an insertion of a stop codon in place of a serine in the amino acid 1016 (Ser1016Stop—Fig 3B). Noteworthy, disruptive mutations in this gene are known to confer resistance to miltefosine in *Leishmania* (Pérez-Victoria *et al*, 2006). Therefore, early adaptation to miltefosine was mainly driven by mutations in LdMT and not by aneuploidy modulations.

Figure 3. Flash selection with miltefosine.

- A Bulk aneuploidy profile of the populations kept under different concentrations of miltefosine (four replicates per concentration—MePOP1-4) at passages 1 (upper panel) and passage 9 (bottom panel).
- B Allele frequency of the Gly160Asp and the Ser1016Stop mutations identified in the miltefosine-transporter gene (LdMT) in the drug-exposed populations.
- C Tracing of lineages before (day 0) and after 17 days (passage 1) under selection with 25 μ M miltefosine (MePOP) or with PBS as control (McPOP). Only lineages that reached frequencies higher than 1% in at least one population in the last timepoint (day 17) are colored. Colored labels display the frequency of some lineages at day 0 and day 17.

Source data are available online for this figure.

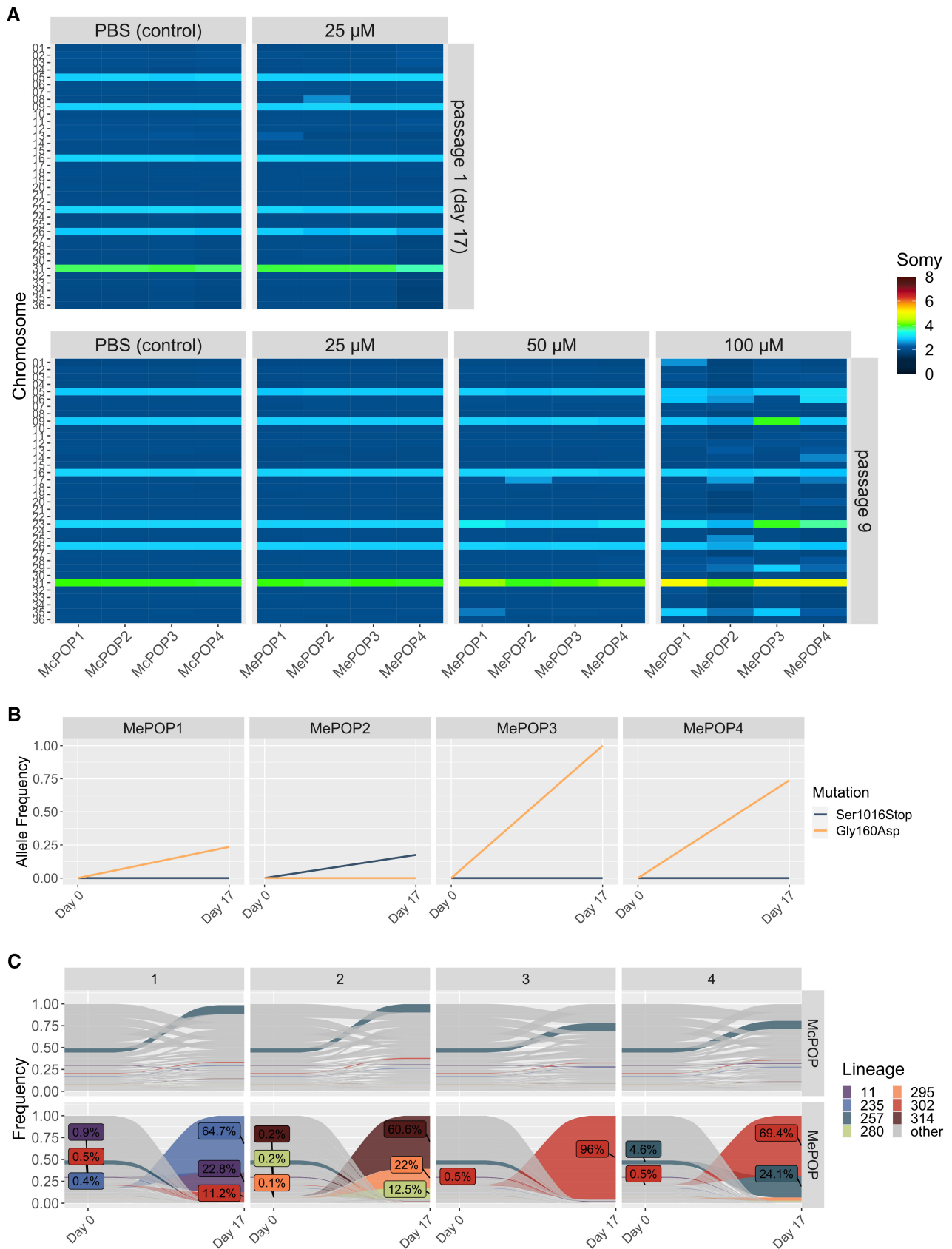


Figure 3.

As the BPK282 population used in the MIL-flash selection was the same barcoded population as in the Sb^{III}-flash selection, we also monitored clonal dynamics between passages 0 (before miltefosine-exposure) and 1 (17 days under miltefosine pressure). This revealed that the bottleneck generated by miltefosine exposure was even stronger than the one associated with Sb^{III} exposure, with only seven lineages surviving in at least one of the MePOP replicates, with one specific lineage (lineage 302) being present in 3 of the 4 replicates (MePOP1, 3 and 4) at passage 1 (Fig 3C). Interestingly, the frequency of lineage 302 in all three replicates where this lineage survived coincided with the allele frequency of the Gly160Asp mutation, suggesting this was a pre-existing mutation present in this lineage. The different mutation seen in MePOP2 also coincides with the fact that this population was dominated by different lineages. The emergence of distinct lineages and mutants in the MePOPs thus illustrate a polyclonal origin of miltefosine resistance in this flash selection experiment.

Aneuploidy dynamics is thus clearly dependent on the nature and strength of the environmental stress. The contrast here observed between the aneuploidy dynamics under Sb^{III} and miltefosine pressure could be explained by two main factors. (i) Aneuploidy changes are not selected under 25–50 μ M miltefosine pressure, because another mechanism can promote survival of the parasites, that is, mutations in LdMT. (ii) The adaptive importance of aneuploidy may also depend on the needed gain or loss of expression for driving drug tolerance. The MRPA is responsible for sequestration of Sb^{III} and a higher expression will increase parasite fitness under drug pressure: this can easily and rapidly be achieved by multiplying the effect of the MRPA amplification already present in BPK282, by increasing the somy of chromosome 23. In contrast, LdMT is responsible for uptake of miltefosine and in this case, a reduction in expression is driving resistance. Here chromosome 13 was already disomic and could probably not further decrease in somy and loss of function was achieved via the SNP ‘path’.

In nature, changes in environmental pressures are often abrupt rather than gradual, and therefore, demand for mechanisms which allow parasite populations to quickly adapt to the new environment. This abrupt change in environments—here represented by our flash selection models—is also a characteristic of drug treatment. In the case of antimonials, measures made in patients treated for visceral leishmaniasis estimate a peak of 10 mg/l or \sim 82 μ M of Sb in the blood after only 2 h post drug administration (Chulay et al, 1988). For miltefosine, blood concentrations can be as high as 70 μ g/ml, or 172 μ M after 72 h (Dorlo et al, 2012). Moreover, bone marrow-derived macrophages exposed to 10 μ M of miltefosine *in vitro* display intracellular concentrations of the drug as high as 323 μ M after 72 h (Voak et al, 2018). This illustrates that *Leishmania* parasites are directly exposed to sharp increases in drug concentrations—in the case of miltefosine, even higher than the concentrations used in this study—in patients upon drug administration.

In conclusion, our data support the role of mosaic aneuploidy in generating multiple pre-adapted karyotypes that can be further modulated *de novo* during drug exposure. This process might depend on the nature and strength of the drug-associated stress and might be potentiated by a stress-induced increase in chromosome instability as seen in other organisms (Chen et al, 2012; Tan et al, 2019; Shen et al, 2020). Further research with longitudinal

SCGS combined with lineage tracing is needed in order to validate these hypotheses. In addition, our studies should be complemented with *in vivo* models, where different environmental stresses can be encountered by the parasite and where the biology of the parasite is different (for instance low replication rate or deep-quiescence; Kloehn et al, 2015; Jara et al, 2019). Finally, the new barcoding method developed and applied here could be used for characterization of clonal dynamics of *Leishmania* in experimental *in vivo* studies.

Materials and Methods

Abbreviations

In the present study, different types of samples are being studied and analyzed by bulk or single-cell approaches. To avoid confusion, we list here the main terms used for sample description.

- *SePOP1-4*: Sb^{III} exposed Populations; these are populations of cells that are analyzed by bulk methods (WGS, barcode amplification), with four replicates. Noteworthy, when we refer to the somy of a given chromosome in a SePOP, this represents an average value calculated on the population of sequenced cells; these values can be integers (most cells of that population show this somy) or intermediate (in that case, there are subpopulations with different somy, for instance a somy value of 2.5 may mean that \sim 50% of the population is disomic for that chromosome and \sim 50% is trisomic, or other combinations).
- *MePOP1-4*: idem but with miltefosine exposure.
- *cPOP1-4* and *McPOP1-4*: control populations not exposed to drugs and maintained in parallel to the drug-exposed populations.

Promastigote culture

A clonal promastigote population of the *L. donovani* BPK282/0 strain (MHOM/NP/02/BPK282/0 clone 4) was maintained at 26°C in culture with HOMEM medium (Gibco™) supplemented with 20% of heat-inactivated fetal calf serum with regular passages being performed every 7 days with 1 in 50 dilutions.

Flash selection with Sb^{III}

A single culture of the barcoded BPK282/0 cl4 strain at 10⁶ promastigotes/ml was divided in 2, where one was further diluted to a final concentration of 5 \times 10⁵/ml with medium containing 764 μ M of potassium antimony tartrate (final concentration 382 μ M, in the text referred to as Sb^{III}) and the other was diluted to the same parasite concentration with a medium containing 0.2% of PBS instead (final PBS concentration 0.1%) as control. These two cultures were subsequently aliquoted into 4 culture flasks each, with a final volume of 5 ml per flask. Each culture was subcultured every 7 days for a total of 5 passages by transferring 2.5 \times 10⁶ promastigotes to a new flask containing fresh medium with either 382 μ M Sb^{III} or 0.1% PBS in a final volume of 5 ml. At the end of each passage (day 7), genomic DNA was extracted from \sim 10⁸ parasites per flask using the QIAamp DNA Mini Kit (QIAGEN) for subsequent barcode and WGS.

lineage in the parasite pool. Barcodes were amplified in a two-step PCR approach using the Kapa HiFi HotStart ReadyMix PCR kit (Kapa Biosciences). The first PCR was done with primers NtBCampF and NtBCampR at a final concentration of 10 μ M each in a final volume of 100 μ l per reaction containing \sim 400 ng of the template DNA. This PCR was carried out with an initial denaturation at 95°C for 3 min, followed by 18 cycles of denaturation at 98°C for 20 s, annealing at 65°C for 30 s, and extension at 72°C for 20 s, with a final extension at 72°C for 2 min. The PCRs were purified using 1.45 \times AMPure XP Beads (Beckman Coulter), eluted in 10 μ l of water and directly transferred to a second PCR containing the primers NtIndex-F and NtIndex-R at 10 μ M each in a final volume of 50 μ l. These primers contain the adapters and index sequences needed for Illumina sequencing. The temperature cycle was 95°C for 3 min, followed by 17 cycles of 98°C for 20 s, 65°C for 30 s, and 72°C for 20 s, with a final extension at 72°C for 2 min. The final PCR product was purified once more with 1.45 \times AMPure XP beads and eluted in 20 μ l of the Buffer EB (QIAGEN). The libraries were quantified using the KAPA Library quantification kit (Kapa Biosciences) and were pooled at equimolar ratios in a final concentration of 3 nM. The library pool was sequenced using a IlluminaTM NextSeq 550 sequencer with 2 \times 75 pb reads targeting on average 5 million pair-end reads per sample.

Barcode counting

Sequencing read pairs in which at least one of the reads had an average quality score lower than 20 were removed from downstream analysis. Then, read pairs were merged to form consensus sequences using the FASTP pipeline (Chen *et al*, 2018). The Bar-tender pipeline (Zhao *et al*, 2018) was used to generate the barcode count table, using the pattern “GACAG[29-39]AGCAG”, and allowing for two mismatches. Downstream analyses were done in R. To distinguish barcodes originating from PCR or sequence errors from true barcodes, we submitted one sample (BPK282 population prior to drug exposure) to three independent library preps. After confirming that barcodes appearing in only one or two libraries were always detected at low frequencies, we considered as true barcodes only those found in all three libraries.

SCGS

SCGS was performed using the single-cell CNVTM solution from 10 \times Genomics. Execution of the protocol and bioinformatic analysis were done as previously described (Negreira *et al*, 2021).

Dose–response assay against antimony and miltefosine

Dose–response assays were performed as previously described (Kulshrestha *et al*, 2013). In summary, logarithmic-stage promastigotes were seeded in 96-well plates at final concentration of 10⁵ parasites per well in supplemented HOMEM medium per well. Parasites were exposed to different concentrations of miltefosine ranging from 3 to 75 μ M (first attempt) or 150 μ M (second attempt). An extra row of wells was kept with 0.2% PBS instead of antimony as a control. Parasites were exposed to the drug for 3 days at 26°C. Afterwards, each plate received 20 μ g/ml of resazurin and was further incubated for 4 h at 26°C. Then, light absorption was measured

at 560 nm/590 nm excitation/emission Using a Victor X2 luminometer. Assays were independently performed 3 times, with three identical plates in each execution serving as technical replicates. When possible, half maximal inhibitory concentrations (IC50) were calculated with GraphPad Prism using a sigmoidal dose–response model with variable slope.

Data availability

Raw sequencing data have been deposited in BioProject (NCBI) with accession number PRJNA970809. Custom scripts used for analysis of barcode and WGS data are available at <https://github.com/gabrielnegreira/LeishBarSeqAndAneuploidy>. Scripts for single-cell data are available at <https://github.com/gabrielnegreira/scgs-somy>. All data are available in the main text or the supplementary materials.

Expanded View for this article is available [online](#).

Acknowledgements

Flemish Ministry of Science and Innovation [Secondary Research Funding ITM—SOFI, Grant MADLEI]. Flemish Fund for Scientific Research [FWO, post-doctoral grant to FvdB].

Author contributions

Gabriel H Negreira: Conceptualization; formal analysis; investigation; visualization; methodology; writing – original draft; writing – review and editing. **Robin de Groote:** Investigation. **Dorien Van Giel:** Investigation. **Pieter Monsieurs:** Data curation; formal analysis; visualization; writing – review and editing. **Ilse Maes:** Investigation. **Geraldine de Muylder:** Conceptualization; methodology; writing – review and editing. **Frederik Van den Broeck:** Conceptualization; funding acquisition; writing – review and editing. **Jean-Claude Dujardin:** Conceptualization; supervision; funding acquisition; writing – original draft; writing – review and editing. **Malgorzata A Domagalska:** Conceptualization; data curation; formal analysis; supervision; funding acquisition; methodology; writing – original draft; writing – review and editing.

Disclosure and competing interests statement

The authors declare that they have no conflict of interest.

References

- Bhang HEC, Ruddy DA, Radhakrishna VK, Caushi JX, Zhao R, Hims MM, Singh AP, Kao I, Rakiec D, Shaw P *et al* (2015) Studying clonal dynamics in response to cancer therapy using high-complexity barcoding. *Nat Med* 21: 440–448
- Brotherton M-C, Bourassa S, Leprohon P, Légaré D, Poirier GG, Droit A, Ouellette M (2013) Proteomic and genomic analyses of antimony resistant *Leishmania infantum* mutant. *PLoS ONE* 8: e81899
- Bussotti G, Gouzou E, Boité MC, Kherachi I, Harrat Z, Eddaikra N, Mottram JC, Antoniou M, Christodoulou V, Bali A *et al* (2018) *Leishmania* genome dynamics during environmental adaptation reveal strain-specific differences in gene copy variation, karyotype instability, and telomeric amplification. *mBio* 9: 1–18
- Bussotti G, Piel L, Pescher P, Domagalska MA, Rajan KS, Cohen-Chalamish S, Doniger T, Hiregange D-G, Myler PJ, Unger R *et al* (2021) Genome

- instability drives epistatic adaptation in the human pathogen *Leishmania*. *Proc Natl Acad Sci USA* 118: e2113744118
- Chen G, Bradford WD, Seidel CW, Li R (2012) Hsp90 stress potentiates rapid cellular adaptation through induction of aneuploidy. *Nature* 482: 246–250
- Chen S, Zhou Y, Chen Y, Gu J (2018) Fastp: an ultra-fast all-in-one FASTQ preprocessor. *Bioinformatics* 34: i884–i890
- Chulay JD, Fleckenstein L, Smith DH (1988) Pharmacokinetics of antimony during treatment of visceral leishmaniasis with sodium stibogluconate or meglumine antimoniate. *Trans R Soc Trop Med Hyg* 82: 69–72
- Chunduri NK, Storchová Z (2019) The diverse consequences of aneuploidy. *Nat Cell Biol* 21: 54–62
- Clayton C (2019) Regulation of gene expression in trypanosomatids: living with polycistronic transcription. *Open Biol* 9: 190072
- Cuypers B, Meysman P, Erb I, Bittremieux W, Valkenburg D, Baggerman G, Mertens I, Sundar S, Khanal B, Notredame C et al (2022) Four layer multi-omics reveals molecular responses to aneuploidy in *Leishmania*. *PLoS Pathog* 18: e1010848
- Domagalska MA, Imamura H, Sanders M, Van Den Broeck F, Bhattarai NR, Vanaerschot M, Maes I, D'Haenens E, Rai K, Rijal S et al (2019) Genomes of *Leishmania* parasites directly sequenced from patients with visceral leishmaniasis in the Indian subcontinent. *PLoS Negl Trop Dis* 13: e0007900
- Dorlo TPC, Balasegaram M, Beijnen JH, de Vries PJ (2012) Miltefosine: a review of its pharmacology and therapeutic efficacy in the treatment of leishmaniasis. *J Antimicrob Chemother* 67: 2576–2597
- Douanne N, Wagner V, Roy G, Leprohon P, Ouellette M, Fernandez-Prada C (2020) MRPA-independent mechanisms of antimony resistance in *Leishmania infantum*. *Int J Parasitol Drugs Drug Resist* 13: 28–37
- Dumetz F, Imamura H, Sanders M, Seblova V, Myskova J, Pescher P, Vanaerschot M, Meehan CJ, Cuypers B, De Muylder G et al (2017) Modulation of aneuploidy in *Leishmania donovani* during adaptation to different *in vitro* and *in vivo* environments and its impact on gene expression. *mBio* 8: e00599–e00517
- Dumetz F, Cuypers B, Imamura H, Zander D, D'Haenens E, Maes I, Domagalska MA, Clos J, Dujardin J-C, De Muylder G (2018) Molecular preadaptation to antimony resistance in *Leishmania donovani* on the Indian subcontinent. *mSphere* 3: e00548-17
- Frézard F, Monte-Neto R, Reis PG (2014) Antimony transport mechanisms in resistant leishmania parasites. *Biophys Rev* 6: 119–132
- Hefnawy A, Negreira G, Jara M, Cotton JA, Maes I, D'Haenens E, Imamura H, Cuypers B, Monsieurs P, Mouchtoglou C et al (2022) Genomic and phenotypic characterization of experimentally selected resistant *Leishmania donovani* reveals a role for dynamin-1-like protein in the mechanism of resistance to a novel antileishmanial compound. *mBio* 13: e0326421
- Imamura H, Dujardin J-C (2019) A guide to next generation sequence analysis of *Leishmania* genomes. In *Leishmania: methods and protocols*, Clos J (ed), pp 69–94. New York, NY: Humana Press
- Imamura H, Downing T, Van den Broeck F, Sanders MJ, Rijal S, Sundar S, Mannaert A, Vanaerschot M, Berg M, De Muylder G et al (2016) Evolutionary genomics of epidemic visceral leishmaniasis in the Indian subcontinent. *eLife* 5: e12613
- Ippolito MR, Martis V, Martin S, Tjihuis AE, Hong C, Wardenaar R, Dumont M, Zerbib J, Spierings DCJ, Fachinetti D et al (2021) Gene copy-number changes and chromosomal instability induced by aneuploidy confer resistance to chemotherapy. *Dev Cell* 56: 2440–2454.e6
- Jara M, Maes I, Imamura H, Domagalska MA, Dujardin JC, Arevalo J (2019) Tracking of quiescence in *Leishmania* by quantifying the expression of GFP in the ribosomal DNA locus. *Sci Rep* 9: 18951
- Kloehn J, Saunders EC, O'Callaghan S, Dagley MJ, McConville MJ (2015) Characterization of metabolically quiescent *Leishmania* parasites in murine lesions using heavy water labeling. *PLoS Pathog* 11: e1004683
- Kulshrestha A, Bhandari V, Mukhopadhyay R, Ramesh V, Sundar S, Maes L, Dujardin JC, Roy S, Salotra P (2013) Validation of a simple resazurin-based promastigote assay for the routine monitoring of miltefosine susceptibility in clinical isolates of *Leishmania donovani*. *Parasitol Res* 112: 825–828
- Leprohon P, Légaré D, Girard I, Papadopoulou B, Ouellette M (2006) Modulation of *Leishmania* ABC protein gene expression through life stages and among drug-resistant parasites. *Eukaryot Cell* 5: 1713–1725
- Mann S, Frasca K, Scherrer S, Henao-Martínez AF, Newman S, Ramanan P, Suarez JA (2021) A review of Leishmaniasis: current knowledge and future directions. *Curr Trop Med Rep* 8: 121–132
- Mannaert A, Downing T, Imamura H, Dujardin J-C (2012) Adaptive mechanisms in pathogens: universal aneuploidy in *Leishmania*. *Trends Parasitol* 28: 370–376
- Monte-Neto R, Laffitte M-CN, Leprohon P, Reis P, Frézard F, Ouellette M (2015) Intrachromosomal amplification, locus deletion and point mutation in the aquaglyceroporin AQP1 gene in antimony resistant *Leishmania (Viannia) guyanensis*. *PLoS Negl Trop Dis* 9: e0003476
- Mulla W, Zhu J, Li R (2014) Yeast: a simple model system to study complex phenomena of aneuploidy. *FEMS Microbiol Rev* 38: 201–212
- Negreira GH, Monsieurs P, Imamura H, Maes I, Kuk N, Yagoubat A, Van den Broeck F, Sterkers Y, Dujardin J-C, Domagalska MA (2021) High throughput single-cell genome sequencing gives insights into the generation and evolution of mosaic aneuploidy in *Leishmania donovani*. *Nucleic Acids Res* 50: 293–305
- Patino LH, Imamura H, Cruz-Saavedra L, Pavia P, Muskus C, Méndez C, Dujardin JC, Ramírez JD (2019) Major changes in chromosomal somy, gene expression and gene dosage driven by SbIII in *Leishmania braziliensis* and *Leishmania panamensis*. *Sci Rep* 9: 9485
- Pérez-Victoria FJ, Sánchez-Cañete MP, Seifert K, Croft SL, Sundar S, Castanys S, Gamarro F (2006) Mechanisms of experimental resistance of *Leishmania* to miltefosine: implications for clinical use. *Drug Resist Updat* 9: 26–39
- Perry MR, Wyllie S, Prajapati VK, Feldmann J, Sundar S, Boelaert M, Fairlamb AH (2011) Visceral leishmaniasis and arsenic: an ancient poison contributing to antimonial treatment failure in the Indian subcontinent? *PLoS Negl Trop Dis* 5: e1227
- Perry MR, Wyllie S, Raab A, Feldmann J, Fairlamb AH (2013) Chronic exposure to arsenic in drinking water can lead to resistance to antimonial drugs in a mouse model of visceral leishmaniasis. *Proc Natl Acad Sci USA* 110: 937–19937
- Replogle JM, Zhou W, Amaro AE, McFarland JM, Villalobos-Ortiz M, Ryan J, Letai A, Yilmaz O, Sheltzer J, Lippard SJ et al (2020) Aneuploidy increases resistance to chemotherapeutics by antagonizing cell division. *Proc Natl Acad Sci USA* 117: 576–30576
- Ricke RM, van Deursen JM (2013) Aneuploidy in health, disease, and aging. *J Cell Biol* 201: 11–21
- Rogers MB, Hillel JD, Dickens NJ, Wilkes J, Bates PA, Depledge DP, Harris D, Her Y, Herzyk P, Imamura H et al (2011) Chromosome and gene copy number variation allow major structural change between species and strains of *Leishmania*. *Genome Res* 21: 142–2142
- Shaw CD, Lonchamp J, Downing T, Imamura H, Freeman TM, Cotton JA, Sanders M, Blackburn G, Dujardin JC, Rijal S et al (2016) *In vitro* selection of miltefosine resistance in promastigotes of *Leishmania donovani* from Nepal: genomic and metabolomic characterization. *Mol Microbiol* 99: 148–1148

- Shen L, Wang Y-T, Tang X-X, Zhang K, Wang P-M, Sui Y, Zheng D-Q (2020) Heat shock drives genomic instability and phenotypic variations in yeast. *AMB Express* 10: 146
- Sterkers Y, Lachaud L, Crobu L, Bastien P, Pagès M (2011) FISH analysis reveals aneuploidy and continual generation of chromosomal mosaicism in *Leishmania major*. *Cell Microbiol* 13: 274–283
- Sterkers Y, Lachaud L, Bourgeois N, Crobu L, Bastien P, Pagès M (2012) Novel insights into genome plasticity in eukaryotes: mosaic aneuploidy in *Leishmania*. *Mol Microbiol* 86: 15–23
- Tan Z, Chan YJA, Chua YJK, Rutledge SD, Pavelka N, Cimini D, Rancati G (2019) Environmental stresses induce karyotypic instability in colorectal cancer cells. *Mol Biol Cell* 30: 42–55
- Tůmová P, Uzlíková M, Jurczyk T, Nohýnková E (2016) Constitutive aneuploidy and genomic instability in the single-celled eukaryote *Giardia intestinalis*. *MicrobiologyOpen* 5: 560–574
- Valdivia HO, Reis-Cunha JL, Rodrigues-Luiz GF, Baptista RP, Baldeviano GC, Gerbasi RV, Dobson DE, Pratlong F, Bastien P, Lescano AG et al (2015) Comparative genomic analysis of *Leishmania (Viannia) peruviana* and *Leishmania (Viannia) braziliensis*. *BMC Genomics* 16: 715
- Voak AA, Standing JF, Sepúlveda N, Harris A, Croft SL, Seifert K (2018) Pharmacodynamics and cellular accumulation of amphotericin B and miltefosine in *Leishmania donovani*-infected primary macrophages. *J Antimicrob Chemother* 73: 1314–1323
- Yang F, Teoh F, Tan ASM, Cao Y, Pavelka N, Berman J (2019) Aneuploidy enables cross-adaptation to unrelated drugs. *Mol Biol Evol* 36: 1768–1782
- Yang F, Gritsenko V, Lu H, Zhen C, Gao L, Berman J, Jiang Y (2021) Adaptation to fluconazole via aneuploidy enables cross-adaptation to amphotericin B and Flucytosine in *Cryptococcus neoformans*. *Microbiol Spectr* 9: e00723-21
- Zhao L, Liu Z, Levy SF, Wu S (2018) Bartender: a fast and accurate clustering algorithm to count barcode reads. *Bioinformatics* 34: 739–747



License: This is an open access article under the terms of the [Creative Commons Attribution-NonCommercial-NoDerivs](https://creativecommons.org/licenses/by-nc-nd/4.0/) License, which permits use and distribution in any medium, provided the original work is properly cited, the use is non-commercial and no modifications or adaptations are made.

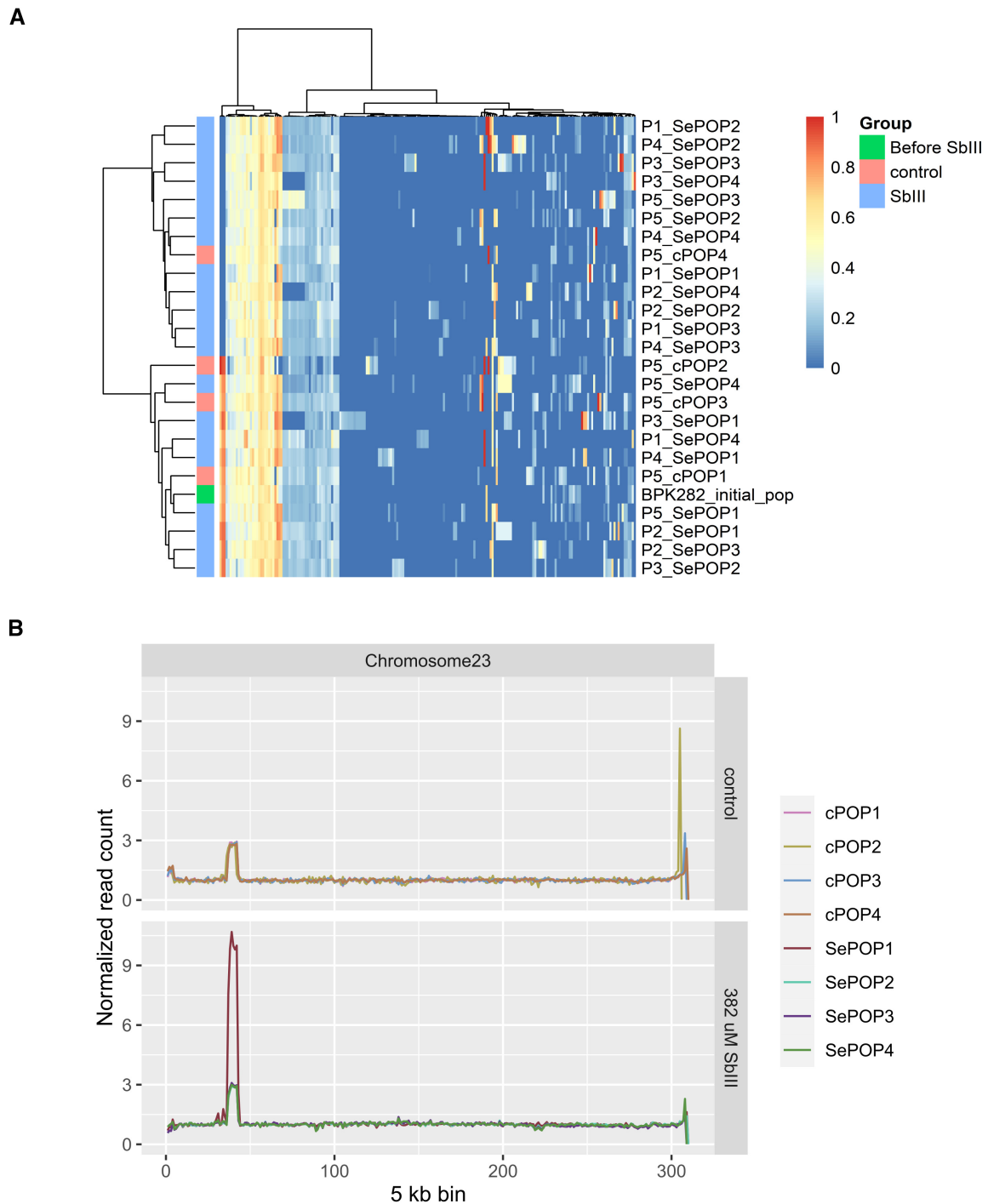


Figure EV2. Additional genomic changes associated with the Sb^{III} -Flash selection performed on the barcoded BPK282 population.

A Heatmap depicting the allele frequencies of SNPs and indels identified in protein coding regions compared to the reference genome. An additional annotation bar display to which group (control or Sb^{III} -exposed) a sample belongs. Samples are named as Px_cPOP_y for controls, and Px_SePOP_y for the Sb^{III} -exposed groups, with x being the number of passages and y being the replicate number. The initial population is named as 'Before Sb^{III} '.

B Copy number variation in the MRPA locus. The Y axis represents the median read count of 5 kb bins normalized by the median count of chromosome 23 and reflects the average copy number per haploid genome of the MRPA locus.

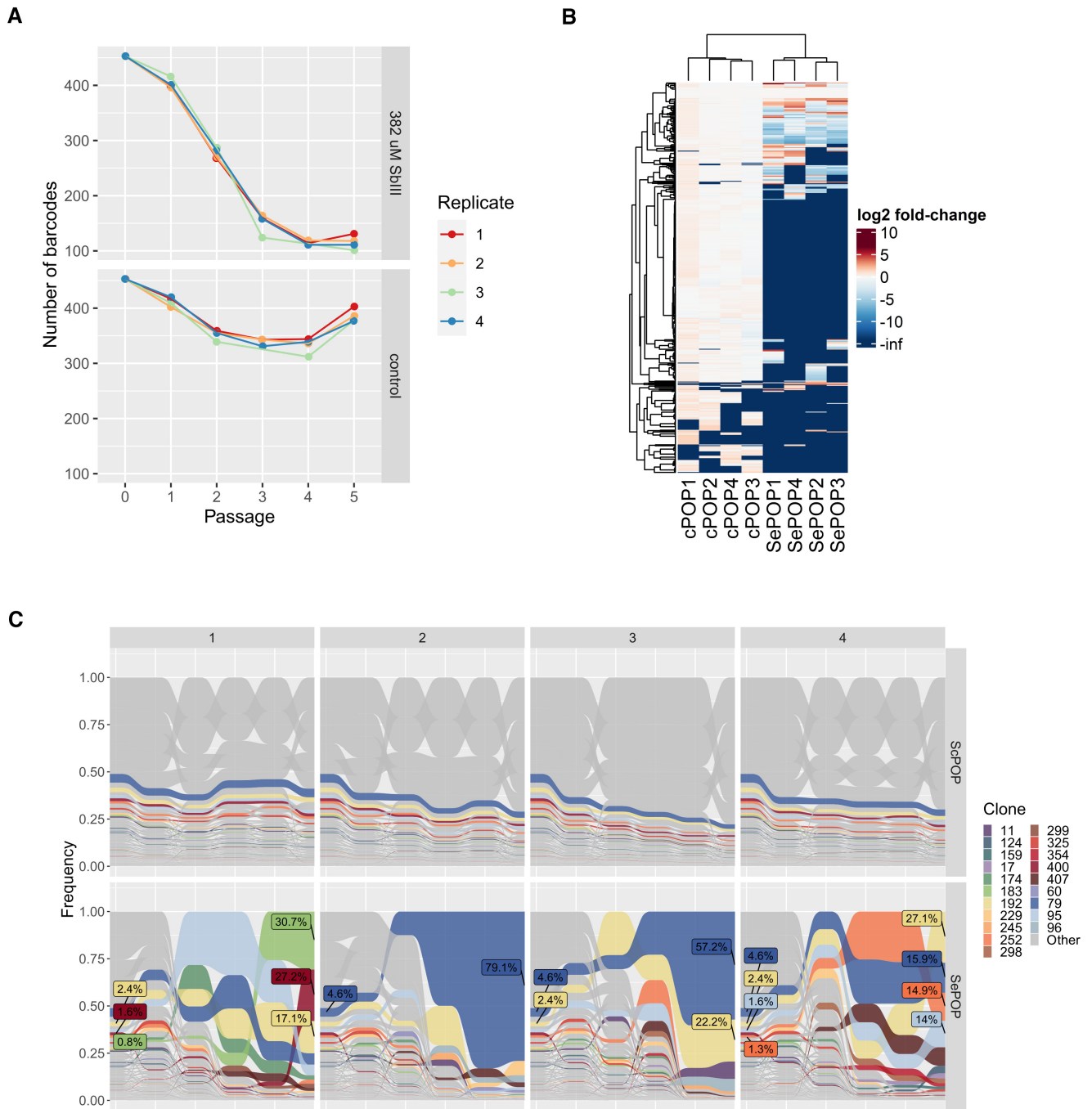


Figure EV3. Supporting figures for main Fig 2.

- A Total number of different barcodes identified in each population at each timepoint in the Sb^{III}-exposed populations (top) and the controls (bottom).
- B Heatmap displaying the Sb^{III}-associated fold-change of each lineage (rows) in each population (columns) at passage 5.
- C Frequency of each barcoded lineage along the 5 passages in the ScPOP1-4 (top) and SePOP1-4 (bottom) populations. This is similar to main Fig 2F but includes the ScPOP1-4 for comparison. Only lineages that reached a frequency higher than 1% at passage 5 in at least one of the SePOP populations are colored.

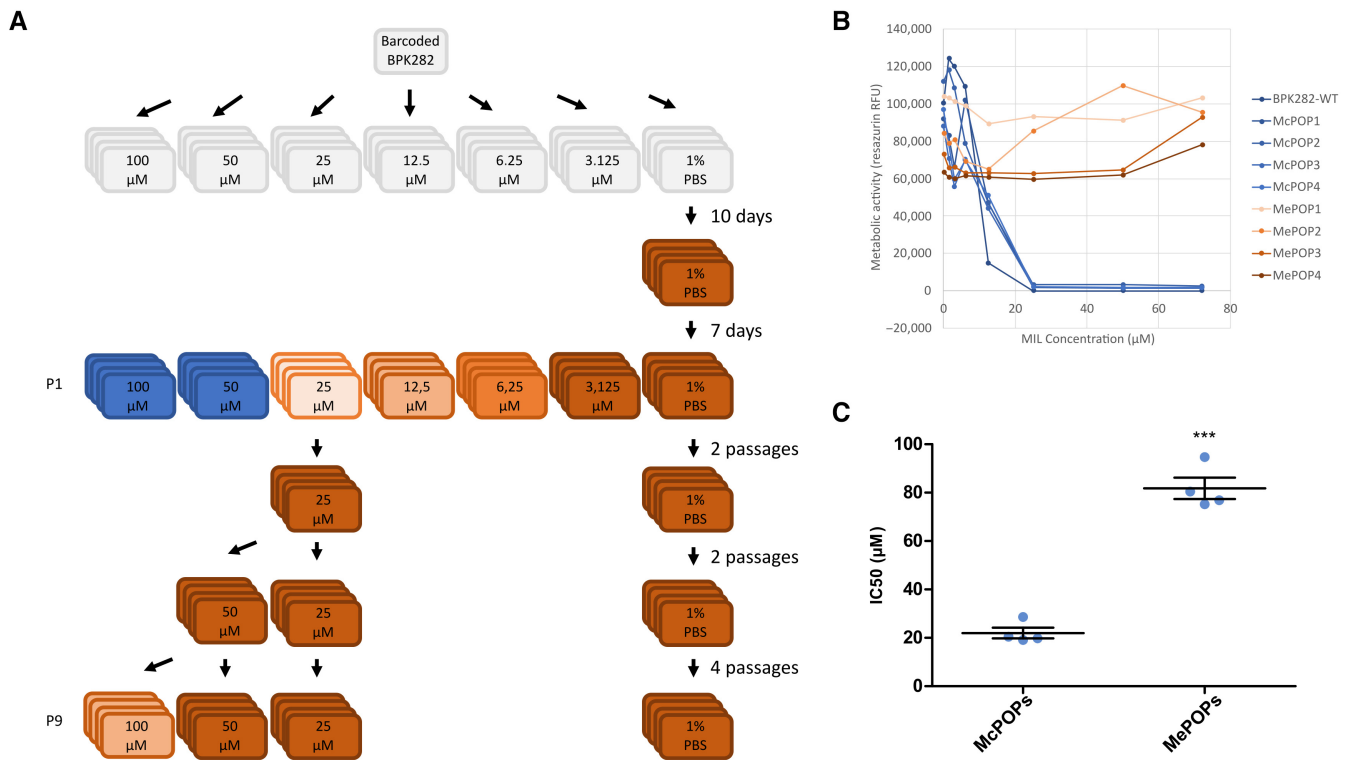


Figure EV4. Supporting figures for flash selection with miltefosine.

- A Schematic representing the experimental design. Colors indicate the lack of viable parasites (blue) or the relative observed number of parasites at day 7 compared to the controls (darker brown = more cells).
- B Dose–response to miltefosine of the metabolic activity of the populations at the first passage after exposure to the drug, estimated with the resazurin assay.
- C Difference in IC₅₀ of the same populations one passage later. *** $P < 0.001$ (t -test).